

## A ROBUST SINGLE CELL RNA-SEQ MANIFOLD

# A robust nonlinear low-dimensional manifold for single cell RNA-seq data

**Archit Verma**

ARCHITV@PRINCETON.EDU

*Department of Chemical and Biological Engineering  
Princeton University  
Princeton, NJ 08544, USA*

**Barbara E. Engelhardt**

BEE@PRINCETON.EDU

*Department of Computer Science  
Center for Statistics and Machine Learning  
Princeton University  
Princeton, NJ 08540, USA*

**Editor:**

## Abstract

Modern developments in single cell sequencing technologies enable broad insights into cellular state. Single cell RNA sequencing (scRNA-seq) can be used to explore cell types, states, and developmental trajectories to broaden understanding of cell heterogeneity in tissues and organs. Analysis of these sparse, high-dimensional experimental results requires dimension reduction. Several methods have been developed to estimate low-dimensional embeddings for filtered and normalized single cell data. However, methods have yet to be developed for unfiltered and unnormalized count data. We present a nonlinear latent variable model with robust, heavy-tailed error and adaptive kernel learning to estimate low-dimensional nonlinear structure in scRNA-seq data. Gene expression in a single cell is modeled as a noisy draw from a Gaussian process in high dimensions from low-dimensional latent positions. This model is called the Gaussian process latent variable model (GPLVM). We model residual errors with a heavy-tailed Student's t-distribution to estimate a manifold that is robust to technical and biological noise. We compare our approach to common dimension reduction tools to highlight our model's ability to enable important downstream tasks, including clustering and inferring cell developmental trajectories, on available experimental data. We show that our robust nonlinear manifold is well suited for raw, unfiltered gene counts from high throughput sequencing technologies for visualization and exploration of cell states.

**Keywords:** Manifold Learning, Gaussian Process Latent Variable Model, cell types, Single Cell RNA-Sequencing (scRNA-seq), Robust Statistics

## 1. Background

High-throughput single cell RNA sequencing (scRNA-seq) is a powerful tool for cataloguing cell types and cell states, and investigating changes in expression over cell developmental trajectories. Droplet-based methods encapsulate individual cells with unique barcode tags that are ligated to cellular RNA fragments (Zheng et al., 2017). Sequenced reads are mapped to both a gene and a cell, creating a high-dimensional cell by gene count matrix—

with hundreds to millions of cells and twenty thousand genes per human cell. These cell by gene count matrices contain a substantial proportion of zeros because of low coverage sequencing per cell (i.e., *dropout*), and also contain substantial variance from both technical and biological sources of noise (Buellner et al.). Computational tools for analyzing scRNA-seq results thus require initial dimension reduction to a lower dimensional manifold capturing gene expression patterns for regularization and computational efficiency. Dimension reduction techniques are conducive to noise reduction (Buellner et al.; Eraslan et al., 2018), sub-population identification (Pierson and Yau; Haghverdi et al., 2016), visualization (Amodio et al.; Van Der Maaten and Hinton), pseudotemporal ordering of development stages (Ahmed et al., 2018; Trapnell et al.; Lönnberg et al., 2017), and imputation (Li and Li, 2018). Lower-dimensional mappings also provide convenient visualizations that inform analytic methods and future experiments.

Linear dimension reduction techniques are commonly used as a first step to downstream analyses. Principal component analysis (Hotelling, 1933) (PCA) – the projection of a high dimensional space onto orthogonal bases that capture the directions of greatest variance – is the first step of several scRNA-seq analysis packages such as PAGODA (Fan et al., 2016) and Waterfall (Shin et al.). Zero-Inflated Factor Analysis (Pierson and Yau) (ZIFA) extends the factor analysis (Harman, 1960) paradigm of a linear mapping onto low dimensional latent dimensions to allow dropouts modeled by Bernoulli random variables to account for the excess of zero counts in scRNA-seq data. Independent component analysis (Comon, 1994) (ICA), which assumes non-Gaussian observations, and canonical correlation analysis (Hotelling, 1936) (CCA), which allows for multiple observations, have also been used as dimension reduction techniques for studying cell developmental trajectories (Trapnell et al.) and for experimental batch correction (Butler et al.).

More sophisticated models eschew the linearity assumption to find richer nonlinear structure in the data. The t-distributed Stochastic Neighbors Embedding (t-SNE) (Van Der Maaten and Hinton) is a popular visualization tool. t-SNE computes the similarity between two points in high dimensional space with respect to a Gaussian kernel distance metric, and estimates a lower dimensional mapping with similarity with respect to a Student's t-distribution metric that minimizes the Kullback-Leibler divergence between the similarity distributions in high and low dimensions. The Gaussian kernel in t-SNE includes a perplexity parameter that controls the decay rate of similarity across the distance between cells. Diffusion maps, used in packages such as Destiny (Angerer et al., 2016), are another tool for nonlinear low dimensional mapping that perform linear decomposition on a kernel similarity matrix of high dimensional observations. SAUCIE (Amodio et al.) implements a variational autoencoder, or a deep neural network that compresses data with the goal of creating an optimal reconstruction from the compressed representation, to execute several single cell tasks. Similarly, scVI (Lopez et al.) uses deep neural networks to create a probabilistic representation in latent space for batch correction, visualization, clustering, and differential expression. One Bayesian probabilistic technique is the Gaussian process latent variable model (Titsias and Lawrence; Lawrence) (GPLVM), which is used by sclVM (Buellner et al.) for noise reduction, and GPfates (Lönnberg et al., 2017) and GrandPrix (Ahmed et al., 2018) for pseudotemporal ordering. The GPLVM models observations (i.e., cells) as draws from Gaussian processes representations of lower dimensional latent variables.

## A ROBUST SINGLE CELL RNA-SEQ MANIFOLD

While current methods for dimension reduction have been successful with early sequencing experiments and filtered expression data, they are limited in their capacity to accurately represent and inform analyses of raw, high throughput sequencing experiments. Linear methods such as PCA and ZIFA are ill-suited for capturing highly nonlinear biological processes across developmental phase, and many implementations scale poorly with increased sample size. Current non-linear methods are highly sensitive parameter choices, including perplexity for t-SNE, kernel variables for diffusion maps, and network architecture for VAEs. Latent dimensions of t-SNE have no global structure, making embedded positions difficult to interpret and leading to uninformative mappings beyond two dimensions. Downstream analyses of t-SNE results are hindered by an inability to map back to observation space. VAEs, like most neural networks, require tens to hundreds of thousands of cells for accurate estimation, which may not be available in smaller experiments. Current methods, particularly those using the GPLVM, work only with filtered, normalized data and incorporate prior information to facilitate the latent mapping.

Robust statistical methods are a natural solution to modeling noisy, sparse count data. We introduce the t-Distributed Gaussian Process Latent Variable Model (tGPLVM) for learning a low dimensional embedding of unfiltered count data. We introduce three features to the basic GPLVM: 1) a robust Student's t-Distribution noise model; 2) a weighted sum of non-smooth covariance kernel functions with parameters estimate from the data; 3) sparse kernel structure. The heavy tailed Student's t-Distribution improves robustness to outliers, previously demonstrated in Gaussian process regression (Tang et al.; Vanhatalo et al.). Matérn kernels have been successfully used in time series modeling to capture non-smooth trajectories (Ahmed et al., 2018). The sparse kernel structure allows us to effectively reduce the number latent dimensions based on the actual complexity of the data. Our implementation of tGPLVM accepts sparse inputs produced from high-throughput experimental cell by gene count matrices.

We demonstrate tGPLVM's ability to estimate informative manifolds from noisy, raw single cell count matrices and highlight its applicability to multiple downstream tasks. We show improved cell type identification via clustering on the estimated latent space using a data set of cerebral cortex cells labeled with estimated cell type (Pollen et al.). We find that the tGPLVM manifold can learn pseudotemporal ordering from a batch of *Plasmodium*-infected mouse cells sequenced across time post exposure (Lönnberg et al., 2017). Finally, we demonstrate that tGPLVM can be used on unprocessed, unnormalized count data from recent high-throughput sequencing methods (Zheng et al., 2017) and used to explore gene expression across cell states. We implement a scalable inference algorithm that can fit hundreds of thousands to millions of cells.

## Results

The t-distributed Gaussian process latent variable model is a nonlinear latent variable model that captures high dimensional observations in low dimensional nonlinear latent space. Expression of each of  $P$  genes across all cells is modeled as a draw from a multivariate normal distribution with the covariance a function of the low-dimensional, latent positions. The observation error is modeled with a heavy tailed Student's t-Distribution with four degrees of freedom to robustly account for variance in the count data due to technical and

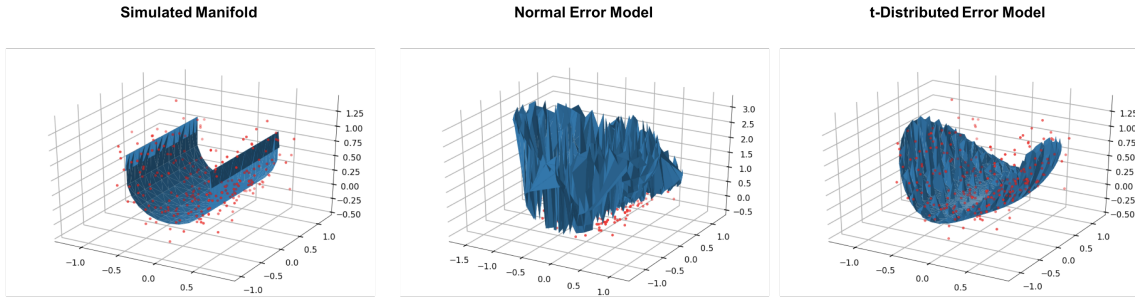


Figure 1: Comparison of error models on the same observations (red) in a multidimensional Gaussian process. Data are simulated from a smooth manifold with t-distributed error (left). A normally distributed error model (center) overfits to the data and fails to find the manifold structure due to the outliers as compared to the manifold estimated by a GP with t-distributed error (right).

biological noise relative to a normally distributed error model (O'Hagan, 1979, 1988). Here, we use a weighted sum of Matérn 1/2, Matérn 3/2, Matérn 5/2, and squared exponential kernel functions to model non-smooth manifolds.

### Nonparametric manifold learning improves cell type identification.

First, we evaluated the ability of tGPLVM and commonly used single cell dimension reduction methods to distinguish distinct cell types. tGPLVM, PCA, ZIFA, and t-SNE were used to map cells labeled with their inferred cell type from the Pollen data (Pollen et al.) to latent spaces varying from two to nine dimensions. With more than two latent dimensions, tGPLVM produced clusters that best corresponded to the actual cell type labels of the four methods (Figure 2). Including Matérn kernels in tGPLVM improves cell type separation in the latent space as measured by normalized mutual information and adjusted rand score (Supplementary Figure 1). Inclusion of Matérn kernels also reduces the uncertainty of posterior estimates of the latent embedding as measured by the average scale parameter of the latent position (Supplementary Figure 2). These results suggest that a robust Bayesian nonparametric manifold is superior to current dimension reduction algorithms for identifying and visualizing distinct cell types captured by scRNA-seq experiments.

### Nonparametric manifold learning can reconstruct development time scales without prior information

Next we test the flexibility of tGPLVM to continuous cellular developmental trajectories by fitting latent mappings for a batch of mouse Th1 and Tfh cells sequenced over seven days after infection with *Plasmodium* (Lönnberg et al., 2017). Visually, we find that the latent mapping from tGPLVM represents the temporal relationships accurately, with most cells positioned among cells from the same or adjacent time points. We build a minimum spanning tree on the latent mappings to infer developmental trajectories. For a two dimensional mapping, only tGPLVM accurately spans the first time point (day 0) to the final time point

## A ROBUST SINGLE CELL RNA-SEQ MANIFOLD

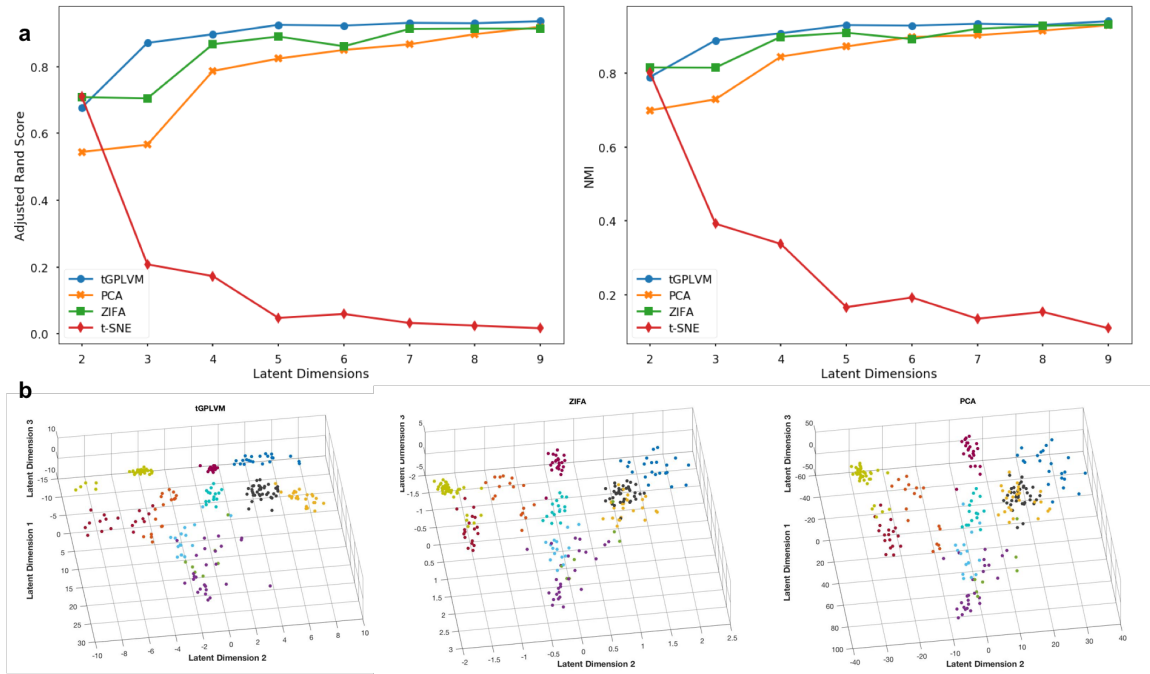


Figure 2: Comparison of manifold learning methods on 11 neural and blood cell populations (Pollen et al.). (a) Average ARS (left) and NMI (right) of ten K-means cluster labels versus available cell type labels with respect to the number of latent dimensions. (b) Three dimensional latent mappings from tGPLVM, PCA, and ZIFA colored by inferred cell type label. t-SNE (not pictured) collapses in three dimensions.

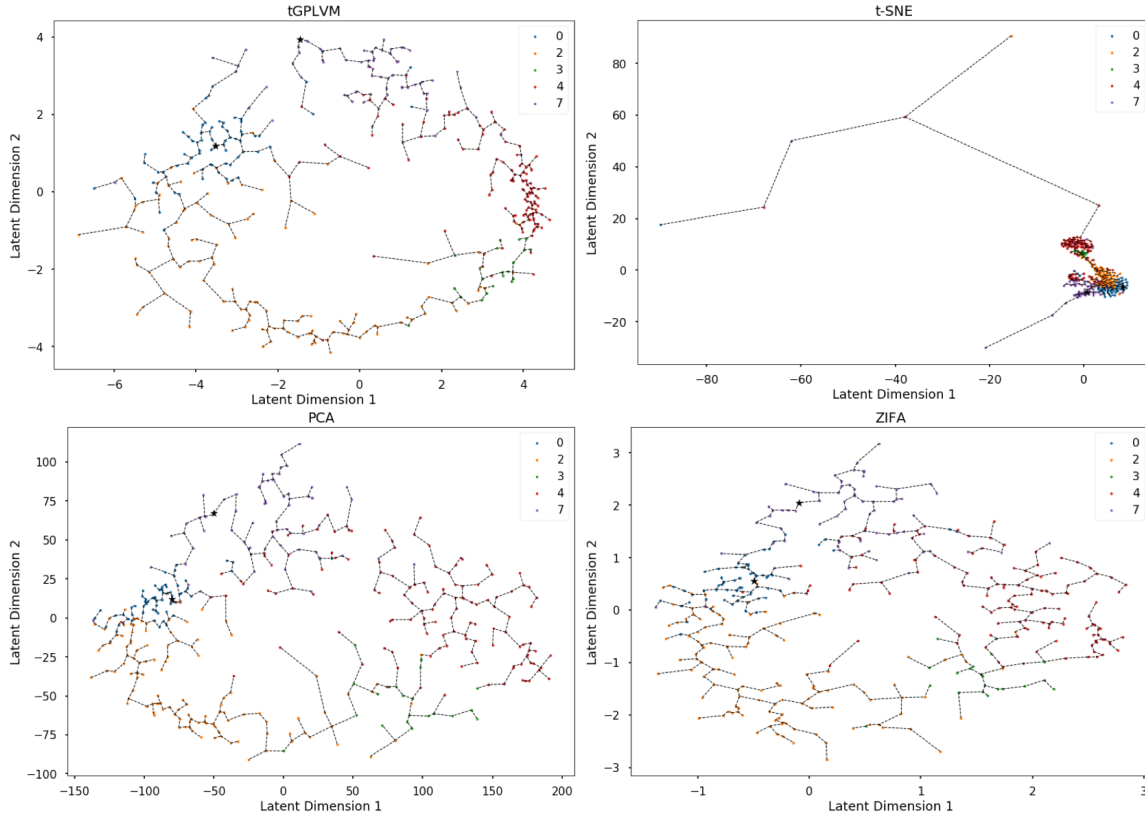


Figure 3: Comparison of manifold learning Methods on *Plasmodium*-infected Th1 and Tfh cells (Lönnberg et al., 2017): Plot of two dimensional latent mapping from tGPLVM, PCA, ZIFA, and t-SNE. Labels indicate days after infection prior to sequencing. Dotted lines represent connections along the minimum spanning tree.

## A ROBUST SINGLE CELL RNA-SEQ MANIFOLD

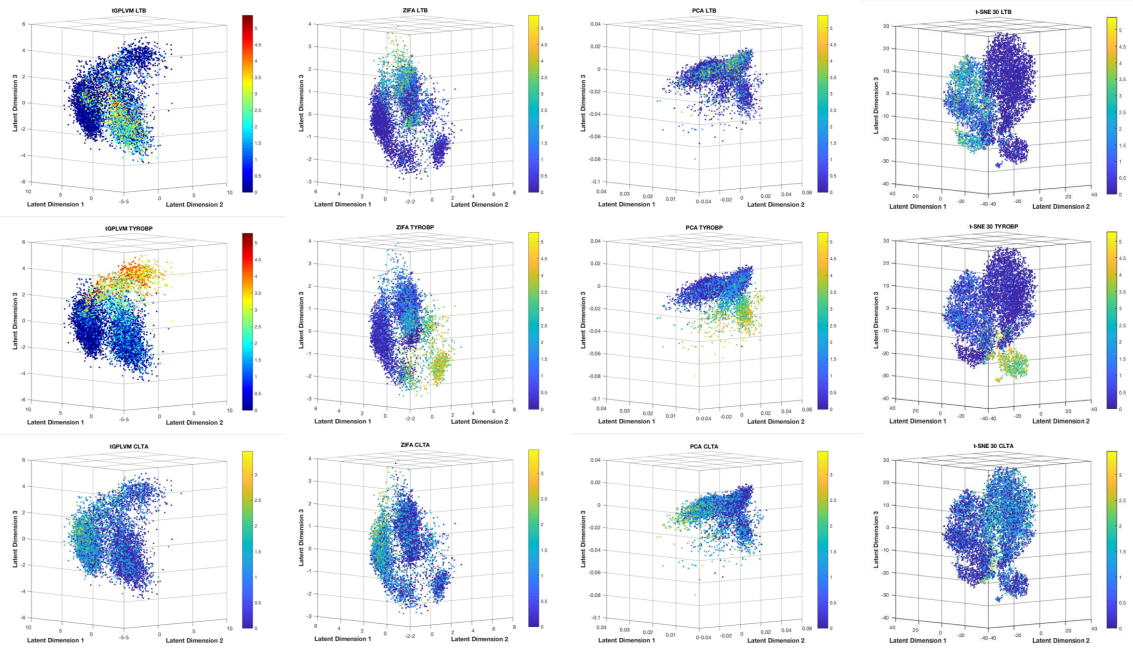


Figure 4: Manifold learning methods on unprocessed CD34+ PBMCs (Zheng et al., 2017) counts. tGPLVM shows the best separation of expression patterns based on cell state marker genes. Color bars indicate  $\log_2(1 + Y)$ , where  $Y$  represents total counts per gene per cell.

(day 7). PCA, ZIFA, and alternate GPLVM models with different error or kernel choices find endpoints of the tree in days 2 or 4. t-SNE is able to separate cells based on time but does not accurately reconstruct the ordering and is clearly sensitive to outliers (Figure 3). This suggests that tGPLVM is a superior dimension reduction technique for identifying developmental pathways in unlabeled settings.

### Nonparametric manifold learning improves visualization of raw count data and captures cell state

Next, we tested tGPLVM’s performance on unfiltered count data. Models were fit on  $\sim 10,000$  CD34+ peripheral blood mononuclear cells (PBMCs) sequenced on a high throughput parallel 10x system (Zheng et al., 2017). Each model was able to find three distinct regions based on expression patterns (Figure 4). PCA is dominated by total counts, with cells with more reads moving further away in latent space, and more frequent cell types dominate the space (Engelhardt and Stephens, 2010). CD34 is a marker for hematopoietic stem cells (Sidney et al., 2014), which differentiate into myeloid and lymphoid cells. From tGPLVM, we can observe this separation from different expression patterns in progenitor cells across dimensions. Dimension three correlates with myeloid cells, demonstrated visually by marker *TYROBP* (Tomasello and Vivier, 2005) (Pearson’s  $r = 0.647$ ; Figure 4), in addition to correlations with macrophage-associated genes (Donato et al.; Xia et al.,

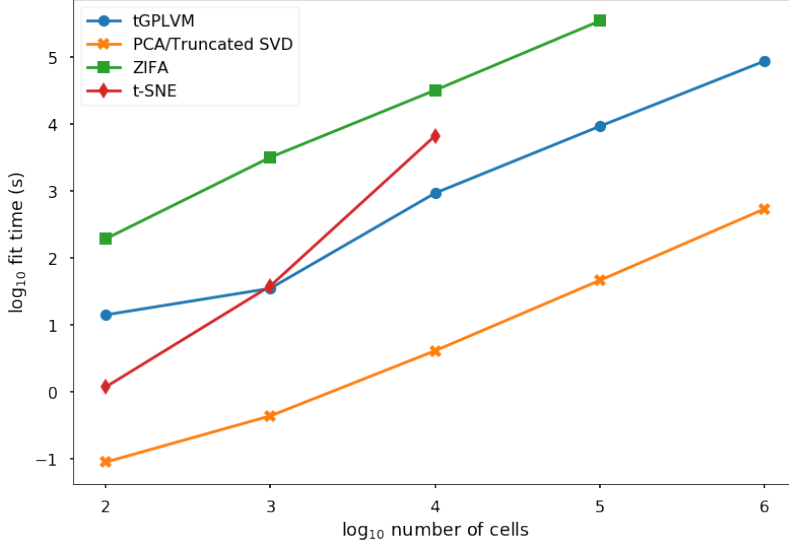


Figure 5: Time to fit a two dimensional embedding vs. sample size on a 16 VCPU, 224 GB memory high performance computing system.

2018) *S100A4* (Pearson's  $r = 0.623$ ) and *S100A6* (Pearson's  $r = 0.665$ ). Dimension two correlates to lymphoid cells, visualized by marker *LTB* (Browning et al., 1993) (Pearson's  $r = 0.306$ ; Figure 4), and further supported by correlation with lymphocyte specific protein-1 *LSP1* (Pearson's  $r = 0.481$ ). Dimension one corresponds to general cellular functions, with strong correlation with mitochondrial activity genes *COX5A* (Pearson's  $r = 0.587$ ) and *STOML2* (Pearson's  $r = 0.474$ ), and shown with *CLTA*, an endocytosis-mediating gene (Stelzer et al., 2016) (Pearson's  $r = 0.461$ ; Figure 4). These distinct expression patterns reflect the broadly different immune cellular functions into which hematopoietic stem cells may develop. Gradients of expression levels projected on tGPLVM embeddings can be used to further interrogate changes in cell states from different experiments and across these manifolds.

### tGPLVM scales to a million cells

Finally, we evaluate the ability of tGPLVM and related methods to fit embeddings for unfiltered, unnormalized, high throughput scRNA-seq data. Models with two latent dimensions were fit on subsamples from 100 to 1 million cells from the 10x 1 million mouse brain cell data (Zheng et al., 2017). tGPLVM and PCA are the only methods that can fit one million cells in a computationally tractable way (Figure 5). ZIFA is slower than tGPLVM by an order of magnitude consistently across sample sizes. Since ZIFA requires a dense input, its input cell count matrix is limited in our framework to approximately 100,000 cells. While t-SNE's implementation can input a sparse matrix format, it does not converge beyond  $10^4$  samples.

To check that the embedding has biological significance, we again used Pearson's correlation to identify genes whose expression is correlated with latent dimensions. We find

A ROBUST SINGLE CELL RNA-SEQ MANIFOLD

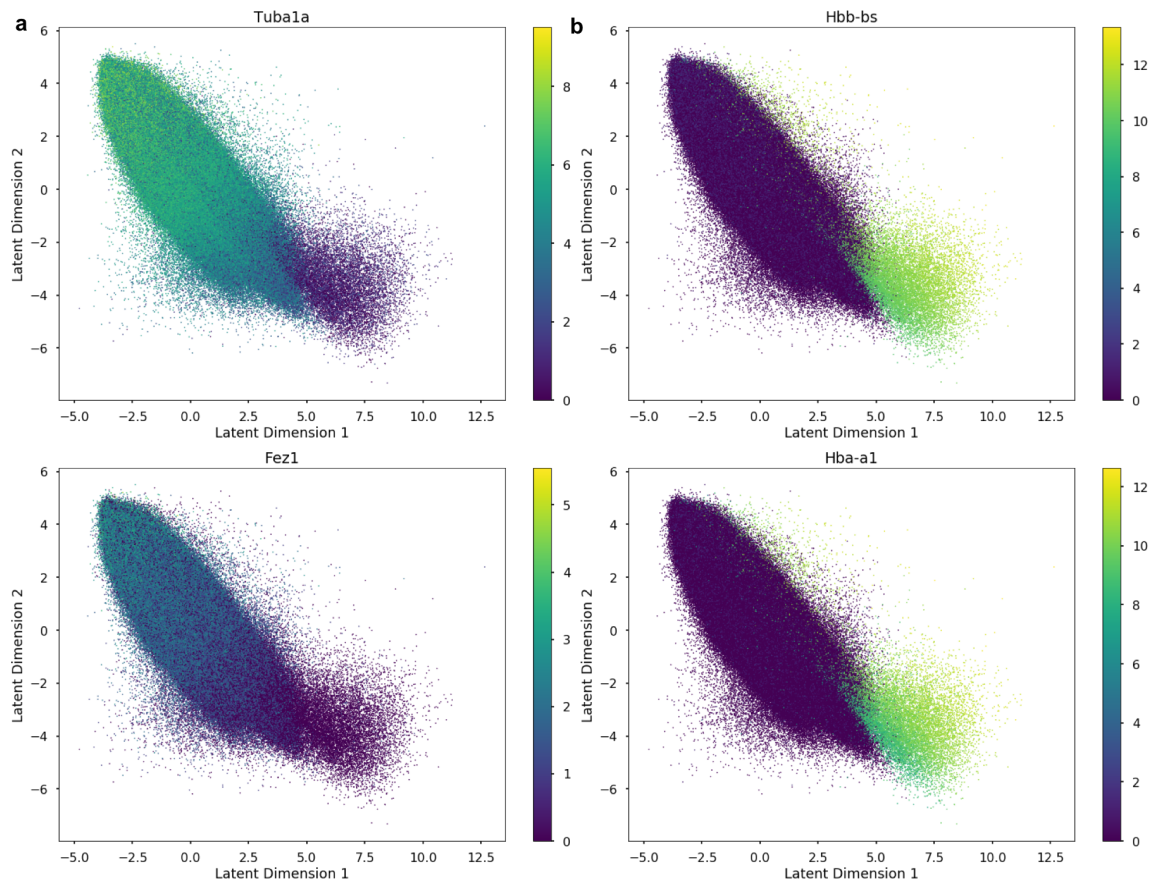


Figure 6: Gene expression patterns across tGPLVM manifold in 1 million mouse brain cells (Zheng et al., 2017). Latent dimension one separates circulatory and blood genes. Latent dimension two is correlated with neural genes. Color bars indicate  $\log_2(1 + Y)$ , where  $Y$  represents total counts per gene per cell.

that latent dimension one corresponds to increased expression of genes associated with the circulatory system and hemoglobin, such as *HBB-BS* (Pearson's  $r = 0.320$ ) and *HBA-A1* (Pearson's  $r = 0.316$ ; Figure 6b). Dimension two correlates with genes such as *TUBA1A* (Pearson's  $r = 0.474$ ) and *FEZ1* (Pearson's  $r = 0.427$ ) that are associated with neural cells (Figure 6a). The ability of tGPLVM to scale to high-throughput data and capture global structure from unnormalized count matrices makes it a powerful method for analyzing future single cell experiments.

## Discussion

We present a Bayesian nonparametric model for robust nonlinear manifold estimation in scRNA-seq settings. tGPLVM captures transcriptional signals in single cell data using a robust Student's t-distribution noise model and integrating adaptive kernel structure in settings with no *a priori* information about clusters or sequencing order. Our results show that tGPLVM is flexible to cell type, cell development, and cell perturbation experiments and can learn informative mappings from filtered and processed data as well as unfiltered raw count data. tGPLVM scales to the size of a million cells as produced by the latest single cell sequencing systems. Despite the sparsity, these data are complex and require several factors to capture variation; we did not use the ARD kernel parameters to remove dimensions for any of our experiments. However, the embedding dimensions in our experiments were able to capture informative representations of these complex data, and as the number of latent dimensions increased some would eventually be removed for being redundant in capturing these complex transcriptional profiles. We expect that the estimated latent mappings can be used for more sophisticated, nonparametric approaches for a variety of single cell tasks from normalization and imputation to cell type identification. We also hope that this robust manifold estimation can be used for other types of data with noisy outliers and sparse features.

## A ROBUST SINGLE CELL RNA-SEQ MANIFOLD

### 1 Methods

#### 2 The t-Distribution Gaussian process latent variable model.

3 The tGPLVM assumes that samples in high dimensional space are noisy observations of  
 4 a Gaussian process of lower dimensional latent features. Let  $Y \in \mathbb{R}^{N \times P}$  represent  $N$   
 5 observations in a high dimensional space of dimension  $P$ , and let  $X \in \mathbb{R}^{N \times Q}$  represent the  
 6 same observations in a lower dimensional space  $Q \ll P$ . Each sample  $x_n$  in  $\{n \in 1, 2, \dots, N\}$   
 7 is assumed to be drawn from a  $Q$  dimensional multivariate normal distribution with identity  
 8 variance:

$$x_i \sim \mathcal{N}_Q(0, I_Q).$$

9 Noiseless observations of each of the  $P$  high dimensional features across  $N$  samples,  $f_p(X)$ ,  
 10 are draws from a zero-mean Gaussian process of  $x$  across a weighted sum of  $M$  kernels:

$$\begin{aligned} f_p(X) &\sim \mathcal{N}_n(0, K_{NN}) \\ k(x, x') &= \sum_{m=1}^M k_m(x, x'), \end{aligned}$$

11 where  $K_{NN}$  represents the  $N \times N$  covariance matrix defined by  $k(x, x')$ . In the traditional  
 12 GPLVM, observations  $y_{n,p}$  are noisy realization of a Normal distribution with mean  $f_{n,p}$   
 13 and variance  $\tau^2$ :

$$y_{n,p}|f_{n,p}(X), \tau^2 \sim \mathcal{N}(f_{n,p}, \tau^2)$$

14 For tGPLVM, each observation  $y_{n,p}$  is drawn from a heavy-tailed Student's t-distribution  
 15 with a set degrees of freedom  $\nu$  and feature-specific variance  $\tau_p^2$  (Tang et al.):

$$\begin{aligned} y_{n,p}|f_{n,p}(X), \tau_p^2, \nu &\sim \text{StudentT}(f_{n,p}, \nu, \tau_p^2) \\ &= \frac{\Gamma((\nu+1)/2)}{\Gamma(\nu/2)\sqrt{\nu\pi}\tau_p} \left(1 + \frac{(y_{n,p} - f_{n,p})^2}{\nu\tau_p^2}\right)^{-(\nu+1)/2}, \end{aligned}$$

16 where we use  $f_{n,p}$  to represent the  $n$ th component of the  $N$  dimensional vector  $f_p(X)$ . We  
 17 set  $\nu = 4$  based on previous work with the supervised Gaussian process with t-distributed  
 18 error (Tang et al.; Vanhatalo et al.).

19 The kernel we use is a flexible sum of an automatic relevance determination (ARD)  
 20 squared exponential kernel and three different Matérn ARD kernels each with hyperparam-  
 21 eters scale  $\sigma_k$  and length scales  $\ell_{k,q}$ . Each ARD dimension-specific length scale,  $\ell_{k,q}$  indicates  
 22 the distance of that latent dimension over which points are similar. Letting  $r$  represent the  
 23 length scale-weighted distance in latent space, the kernels are defined as:

$$\begin{aligned} r &= \sum_{q=1}^Q \frac{(x_q - x'_q)}{\ell_{m,q}} \\ k_1(x, x') &= k_{SE}(x, x') = \sigma_1^2 \exp \left\{ -\frac{1}{2} r^2 \right\} \end{aligned}$$

$$\begin{aligned} k_2(x, x') &= k_{Mat1/2}(x, x') = \sigma_2^2 \exp \{-r\} \\ k_3(x, x') &= k_{Mat3/2}(x, x') = \sigma_3^2(1 + \sqrt{3}r) \exp \left\{ -\sqrt{3}r \right\} \\ k_4(x, x') &= k_{Mat5/2}(x, x') = \sigma_4^2(1 + \sqrt{3}r + \frac{5}{3}r^2) \exp \left\{ -\sqrt{5}r \right\}. \end{aligned}$$

We use Black Box Variational Inference (Ranganath et al.) to estimate the posterior distribution for tGPLVM. We adapt the variational distributions from prior work (Damianou et al., 2016). Inference is implemented in Python using Edward (Tran et al., 2016, 2017). To scale to large data sets, minibatches of both cells and genes are used to approximate gradients at each update. Genes (i.e., features) are sampled in proportion to the percentage of cells in which they are expressed to efficiently approximate the covariance matrix calculated during inference, inspired by previous random matrix algorithms to approximate high dimensional matrix multiplication (Drineas et al.). Cells (i.e., samples) are sampled uniformly in every batch. Inference was performed on Microsoft Azure High Performance Computing cores.

### Single cell RNA-seq data

We chose four data sets to evaluate tGPLVM's applicability to identifying cell type, state, and developmental trajectory and scalability to experiments with large numbers of cells. The Pollen data (Pollen et al.), which were used to evaluate clustering, consist of 11 distinct mouse neural and blood cell populations across 249 cells sequenced on a Fluidigm C1 systems. Pollen is a dense matrix because of high read depth, with about 80% non-zero values. The counts are log normalized as  $\log_{10}(1 + Y)$ . Inference of development trajectories was evaluated on the data used to develop the method GPfates from Lonnberg (Lönnberg et al., 2017). Lonnberg (Lönnberg et al., 2017) sequenced 408 T helper cells cells over 7 days after *Plasmodium* infection on a Fluidigm C1 system. The Lonnberg data are provided as TPM measurements. The data are sparse and normalized by  $\log_2(1 + Y)$ . Cell state was explored on batch of CD34+ peripheral blood mononuclear cells (Zheng et al., 2017) (PBMCs). About 10,000 cells were captured with 10x Cell Ranger sequencing technologies. These sparse data were also normalized as  $\log_2(1 + Y)$ . Finally, to ensure scalability to the most recent experimental data sets, we fit the model to 1 million mice brain cells sequenced on a 10x Cell Ranger (Zheng et al., 2017). We normalized the mice brain cells as  $\log_2(1 + Y)$

### IDENTIFYING CELL TYPES WITH K-MEANS CLUSTERING

Clustering for cell type identification was evaluated on the Pollen (Pollen et al.) data. tGPLVM and comparison methods were used to fit latent mappings between 2 and 9 dimensions. To perform clustering for each of the estimated latent manifolds, we used k-means clustering with the number of clusters equal to the number of different cell type or cell state labels in the existing data. Clustering with k-means was repeated 10 times on the mean of the posterior of the latent position and evaluated against true labels using normalized mutual information (NMI) and adjusted rand score (ARS). Mutual information measures the amount of information contained in one random variable, the true labels, by another random variable, the inferred labels. NMI normalizes mutual information by the geometric mean of the entropy of both labels to a scale of zero - no mutual information - to one - the

## A ROBUST SINGLE CELL RNA-SEQ MANIFOLD

same distribution (Strehl and Ghosh, 2003). ARS is a measure of the proportion of shared members between pairs of true and estimated clusters (Hubert and Arabie). Zero inflated factor analysis (ZIFA) (Pierson and Yau), t-SNE (Van Der Maaten and Hinton) (perplexity set to default 30), and PCA (Hotelling, 1933) were tested as comparison methods. To evaluate the robust adaptations of the tGPLVM model, we fit tGPLVM with only an SE kernel or SE and Matérn 1/2 kernel as well as tGPLVM with normally distributed error.

### TRAJECTORY BUILDING WITH MINIMUM SPANNING TREES

tGPLVM was used to fit a two dimensional latent mappings for the Lonnberg (Lönnberg et al., 2017) developmental data. The minimum spanning tree was found on Euclidean distance matrix of the posterior means of the low dimensional embedding and compared to sequencing time to verify correct ordering. The same analysis was performed with ZIFA (Pierson and Yau), t-SNE (Van Der Maaten and Hinton) (perplexity set to default 30), and PCA (Hotelling, 1933).

### VISUALIZATION OF SPARSE, RAW COUNT MATRICES

tGPLVM was used to fit a three-dimensional mapping for the two 10x data sets, CD34+ cells and mice brain cells. Pearson correlation between latent position posterior mean and expression counts was used to identify genes associated with latent dimensions. ZIFA (Pierson and Yau), t-SNE (Van Der Maaten and Hinton) (perplexity set to default 30), and PCA (truncated SVD (Halko et al.)) were also fit to the CD34+ cell data to compare computational time.

### Scaling inference to high-throughput experiments

Computational times were recorded for samples of 100, 1,000, 10,000, 100,000 and 1,000,000 cells from the 10x 1 million mouse brains cells (Zheng et al., 2017) to a latent embedding using tGPLVM and comparison methods. Experiments were run on a Standard H16m (16 VCPUs, 224 GB memory) Azure high performance computing Unix system. tGPLVM was run for 100 passes through the data. Each minibatch contained the minimum of 2500 or the number of cells and 250 genes. ZIFA, t-SNE, and PCA (using truncated SVD) were fit until convergence or failure.

### Acknowledgments

BEE was funded by CZI AWD1005664, CZI, CZI AWD1005667, NIH R01 HL133218, NIH U01 HG007900, a Sloan Faculty Fellowship, and an NSF CAREER AWD1005627.

The authors declare that they have no competing financial interests.

Correspondence and requests for materials should be addressed to B.E.E. (email: bee@princeton.edu).

Software is available at <https://github.com/architverma1/tGPLVM>

VERMA & ENGELHARDT

**95 Author Contributions**

**96** A.V. and B.E.E designed experiments, analyzed experiments, and wrote paper. A.V. wrote  
**97** implementation and ran experiments.

## A ROBUST SINGLE CELL RNA-SEQ MANIFOLD

### 98 References

- 99 Sumon Ahmed, Magnus Rattray, and Alexis Boukouvalas. Grandprix: Scaling up the  
100 bayesian gplvm for single-cell data. *Bioinformatics*, page bty533, 2018. doi: 10.1093/  
101 bioinformatics/bty533.
- 102 Matthew Amodio, Krishnan Srinivasan, David van Dijk, Hussein Mohsen, Kristina Yim,  
103 Rebecca Muhle, Kevin R Moon, Susan Kaech, Ryan Sowell, Ruth Montgomery, James  
104 Noonan, Guy Wolf, and Smita Krishnaswamy. Exploring Single-Cell Data with Multi-  
105 tasking Deep Neural Networks. *bioRxiv*. doi: 10.1101/237065.
- 106 Philipp Angerer, Laleh Haghverdi, Maren Bttner, Fabian J. Theis, Carsten Marr, and Flo-  
107 rian Buettner. destiny: diffusion maps for large-scale single-cell data in r. *Bioinformatics*,  
108 32(8):1241–1243, 2016. doi: 10.1093/bioinformatics/btv715.
- 109 J L Browning, A Ngam-ek, P Lawton, J DeMarinis, R Tizard, E P Chow, C Hesslon,  
110 B O’Brine-Greco, S Foley, and C F Ware. Lymphotoxin B, a novel member of the TNF  
111 family that forms a heteromeric complexes with lymphotoxin on the cell surface. *Cell*,  
112 72:847–856, 1993.
- 113 Florian Buettner, Kedar N Natarajan, F Paolo Casale, Valentina Proserpio, Antonio Scial-  
114 done, Fabian J Theis, Sarah A Teichmann, John C Marioni, and Oliver Stegle. Compu-  
115 tational analysis of cell-to-cell heterogeneity in single-cell RNA-sequencing data reveals  
116 hidden subpopulations of cells. *Nature Biotechnology*, page 155, jan .
- 117 Andrew Butler, Paul Hoffman, Peter Smibert, Efthymia Papalex, and Rahul Satija. In-  
118 tegrating single-cell transcriptomic data across different conditions, technologies, and  
119 species. *Nature Biotechnology*, page 411, apr .
- 120 Pierre Comon. Independent component analysis, A new concept? *Signal Processing*, 36(3):  
121 287–314, 1994. ISSN 01651684. doi: 10.1016/0165-1684(94)90029-9.
- 122 Andreas C Damianou, Michalis K Titsias, and Neil D Lawrence. Variational inference for  
123 latent variables and uncertain inputs in Gaussian processes. *Journal of Machine Learning  
124 Research*, 17:1–62, 2016. ISSN 15337928.
- 125 R. Donato, B. R. Cannon, G. Sorci, F. Riuzzi, K. Hsu, D. J. Weber, and C. L. Geczy.  
126 Functions of S100 Proteins. *Current Molecular Medicine*, (1):24–57. ISSN 15665240. doi:  
127 10.2174/156652413804486214.
- 128 Petros Drineas, Ravi Kannan, and Michael W. Mahoney. Fast Monte Carlo Algorithms  
129 for Matrices I: Approximating Matrix Multiplication. *SIAM Journal on Computing*, (1):  
130 132–157. ISSN 0097-5397. doi: 10.1137/S0097539704442684.
- 131 Barbara E. Engelhardt and Matthew Stephens. Analysis of population structure: A unifying  
132 framework and novel methods based on sparse factor analysis. *PLoS Genetics*, 6(9), 2010.  
133 ISSN 15537390. doi: 10.1371/journal.pgen.1001117.

- 134 Gökcen Eraslan, Lukas M Simon, Maria Mircea, Nikola S Mueller, and Fabian J Theis.  
135 Single cell RNA-seq denoising using a deep count autoencoder. *bioRxiv*, 2018. doi:  
136 10.1101/300681.
- 137 Jean Fan, Neeraj Salathia, Rui Liu, Gwendolyn E. Kaeser, Yun C Yung, Joseph L Her-  
138 man, Fiona Kaper, Jian-Bing Fan, Kun Zhang, Jerols Chun, and Peter V Kharchenko.  
139 Characterizing transcriptional heterogeneity through pathway and gene set overdispersion  
140 analysis. *Nature Methods*, 13(13):241–244, 2016. ISSN 1548-7105.
- 141 Laleh Haghverdi, Maren Büttner, F. Alexander Wolf, Florian Buettner, and Fabian J. Theis.  
142 Diffusion pseudotime robustly reconstructs lineage branching. *Nature Methods*, 13(10):  
143 845–848, 2016. ISSN 15487105. doi: 10.1038/nmeth.3971.
- 144 Nathan Halko, Per-Gunnar Martinsson, and Joel A. Tropp. Finding structure with ran-  
145 domness: Probabilistic algorithms for constructing approximate matrix decompositions.  
146 pages 1–74. ISSN 0036-1445. doi: 10.1137/090771806.
- 147 Harry H Harman. Modern factor analysis. 1960.
- 148 Harold Hotelling. Analysis of a complex of statistical variables into principal components.  
149 *Journal of educational psychology*, 24(6):417, 1933.
- 150 Harold Hotelling. Relations between two sets of variates. *Biometrika*, 28(3-4):321–377,  
151 1936. doi: 10.1093/biomet/28.3-4.321.
- 152 Lawrence Hubert and Phipps Arabie. Comparing partitions. *Journal of Classification*, (1):  
153 193–218, dec . ISSN 1432-1343. doi: 10.1007/BF01908075.
- 154 Neil Lawrence. Probabilistic non-linear Principal Component Analysis with Gaussian Pro-  
155 cess Latent Variable Models. *Journal of Machine Learning Research*, pages 1783–1816.  
156 ISSN 1476-4687.
- 157 Wei Vivian Li and Jingyi Jessica Li. An accurate and robust imputation method scImpute  
158 for single-cell RNA-seq data. *Nature Communications*, 9(1):997, 2018. ISSN 2041-1723.  
159 doi: 10.1038/s41467-018-03405-7.
- 160 Tapio Lönnberg, Valentine Svensson, Kylie R James, Daniel Fernandez-Ruiz, Ismail Sebina,  
161 Ruddy Montandon, Megan S F Soon, Lily G Fogg, Arya Sheela Nair, Urijah N. Liligeto,  
162 Michael J T Stubbington, Lam-Ha Ly, Frederik Otzen Bagger, Max Zwiessele, Neil D  
163 Lawrence, Fernando Souza-Fonseca-Guimaraes, Patrick T Bunn, Christian R Engwerda,  
164 William R Heath, Oliver Billker, Oliver Stegle, Ashraful Haque, and Sarah A Teichmann.  
165 Single-cell RNA-seq and computational analysis using temporal mixture modeling resolves  
166 T H 1/T FH fate bifurcation in malaria. *Science Immunology*, 2(9):eaal2192, 2017. ISSN  
167 2470-9468. doi: 10.1126/sciimmunol.aal2192.
- 168 Romain Lopez, Jeffrey Regier, Michael B Cole, Michael Jordan, and Nir Yosef. Bayesian  
169 Inference for a Generative Model of Transcriptome Profiles from Single-cell RNA Se-  
170 quencing. *bioRxiv*. doi: 10.1101/292037.

## A ROBUST SINGLE CELL RNA-SEQ MANIFOLD

- 171 A. O'Hagan. On outlier rejection phenomena in bayes inference. *Journal of the Royal  
172 Statistical Society. Series B (Methodological)*, 41(3):358–367, 1979. ISSN 00359246.
- 173 A. O'Hagan. Modelling with heavy tails. In *Bayesian statistics, 3 (Valencia, 1987)*, Oxford  
174 Sci. Publ., pages 345–359. Oxford Univ. Press, New York, 1988.
- 175 Emma Pierson and Christopher Yau. ZIFA: Dimensionality reduction for zero-inflated  
176 single-cell gene expression analysis. *Genome Biology*, (1):241. ISSN 1474-760X. doi:  
177 10.1186/s13059-015-0805-z.
- 178 Alex A Pollen, Tomasz J Nowakowski, Joe Shuga, Xiaohui Wang, Anne A Leyrat, Jan H Lui,  
179 Nianzhen Li, Lukasz Szpankowski, Brian Fowler, Peilin Chen, Naveen Ramalingam, Gang  
180 Sun, Myo Thu, Michael Norris, Ronald Lebofsky, Dominique Toppani, Darnell W Kemp  
181 II, Michael Wong, Barry Clerkson, Brittnee N Jones, Shiquan Wu, Lawrence Knutsson,  
182 Beatriz Alvarado, Jing Wang, Lesley S Weaver, Andrew P May, Robert C Jones, Marc A  
183 Unger, Arnold R Kriegstein, and Jay A A West. Low-coverage single-cell mRNA sequenc-  
184 ing reveals cellular heterogeneity and activated signaling pathways in developing cerebral  
185 cortex. *Nature Biotechnology*, page 1053, aug .
- 186 Rajesh Ranganath, Sean Gerrish, and David M Blei. Black Box Variational Inference.  
187 *Aistats*. ISSN 15337928.
- 188 Jaehoon Shin, Daniel A. Berg, Yunhua Zhu, Joseph Y. Shin, Juan Song, Michael A.  
189 Bonaguidi, Grigori Enikolopov, David W. Nauen, Kimberly M. Christian, Guo Li Ming,  
190 and Hongjun Song. Single-Cell RNA-Seq with Waterfall Reveals Molecular Cascades  
191 underlying Adult Neurogenesis. *Cell Stem Cell*, (3):360–372. ISSN 18759777. doi:  
192 10.1016/j.stem.2015.07.013.
- 193 Laura E. Sidney, Matthew J. Branch, Siobhán E. Dunphy, Harminder S. Dua, and An-  
194 drew Hopkinson. Concise review: Evidence for CD34 as a common marker for diverse  
195 progenitors. *Stem Cells*, 32(6):1380–1389, 2014. ISSN 15494918. doi: 10.1002/stem.1661.
- 196 Gil Stelzer, Naomi Rosen, Inbar Plaschkes, Shahar Zimmerman, Michal Twik, Simon  
197 Fishilevich, Tsippi Iny Stein, Ron Nudel, Iris Lieder, Yaron Mazor, Sergey Kaplan, Dvir  
198 Dahary, David Warshawsky, Yaron Guan-Golan, Asher Kohn, Noa Rappaport, Mari-  
199 lyn Safran, and Doron Lancet. The GeneCards suite: From gene data mining to dis-  
200 ease genome sequence analyses. *Current Protocols in Bioinformatics*, 2016(June):1.30.1–  
201 1.30.33, 2016. ISSN 1934340X. doi: 10.1002/cpbi.5.
- 202 Alexander Strehl and Joydeep Ghosh. Cluster ensembles - A knowledge reuse framework  
203 for combining multiple partitions. *Journal of Machine Learning Research*, 3(3):583–617,  
204 2003. ISSN 15324435. doi: 10.1162/153244303321897735.
- 205 Qingtao Tang, Li Niu, Yisen Wang, Tao Dai, Wangpeng An, Jianfei Cai, and Shu Tao  
206 Xia. Student-t process regression with student-t likelihood. *IJCAI International Joint  
207 Conference on Artificial Intelligence*, pages 2822–2828. ISSN 10450823.
- 208 Michalis Titsias and Neil Lawrence. Bayesian Gaussian Process Latent Variable Model. *Ar-  
209 tificial Intelligence*, pages 844–851. ISSN 0899-7667. doi: 10.1162/089976699300016331.

- 210 Elena Tomasello and Eric Vivier. KARAP/DAP12/TYROBP: Three names and a multi-  
211 plicity of biological functions. *European Journal of Immunology*, 35(6):1670–1677, 2005.  
212 ISSN 00142980. doi: 10.1002/eji.200425932.
- 213 Dustin Tran, Alp Kucukelbir, Adji B. Dieng, Maja Rudolph, Dawen Liang, and David M.  
214 Blei. Edward: A library for probabilistic modeling, inference, and criticism. *arXiv  
215 preprint arXiv:1610.09787*, 2016.
- 216 Dustin Tran, Matthew D. Hoffman, Rif A. Saurous, Eugene Brevdo, Kevin Murphy, and  
217 David M. Blei. Deep probabilistic programming. In *International Conference on Learning  
218 Representations*, 2017.
- 219 Cole Trapnell, Davide Cacchiarelli, and Xiaojie Qiu. Monocle : Cell counting , differential  
220 expression , and trajectory analysis for single-cell RNA-Seq experiments. *Bioconductor*,  
221 page 10.
- 222 L J P Van Der Maaten and G E Hinton. Visualizing high-dimensional data using t-SNE.  
223 *Journal of Machine Learning Research*, pages 2579–2605. ISSN 1532-4435. doi: 10.1007/  
224 s10479-011-0841-3.
- 225 Jarno Vanhatalo, Pasi Jylänki, and Aki Vehtari. Gaussian process regression with Student-t  
226 likelihood. In Y Bengio, D Schuurmans, J D Lafferty, C K I Williams, and A Culotta,  
227 editors, *Advances in Neural Information Processing Systems 22*, pages 1910–1918. Curran  
228 Associates, Inc.
- 229 Chang Xia, Zachary Braunstein, Amelia C. Toomey, Jixin Zhong, and Xiaoquan Rao. S100  
230 proteins as an important regulator of macrophage inflammation. *Frontiers in Immunol-*  
231 *ogy*, 8(JAN):1–11, 2018. ISSN 16643224. doi: 10.3389/fimmu.2017.01908.
- 232 Grace X Y Zheng, Jessica M Terry, Phillip Belgrader, Paul Ryvkin, Zachary W Bent, Ryan  
233 Wilson, Solongo B Ziraldo, Tobias D Wheeler, Geoff P McDermott, Junjie Zhu, Mark T  
234 Gregory, Joe Shuga, Luz Montesclaros, Jason G Underwood, Donald A Masquelier, Ste-  
235 fanie Y Nishimura, Michael Schnall-Levin, Paul W Wyatt, Christopher M Hindson, Rajiv  
236 Bharadwaj, Alexander Wong, Kevin D Ness, Lan W Beppu, H Joachim Deeg, Christo-  
237 pher McFarland, Keith R Loeb, William J Valente, Nolan G Ericson, Emily A Stevens,  
238 Jerald P Radich, Tarjei S Mikkelsen, Benjamin J Hindson, and Jason H Bielas. Massively  
239 parallel digital transcriptional profiling of single cells. *Nature Communications*, 8:14049,  
240 jan 2017.